RSC Advances

PAPER

View Article Online
View Journal | View Issue

Cite this: *RSC Adv.*, 2019, **9**, 2258

Phenylboronic acid derivative-modified (6,5) single-wall carbon nanotube probes for detecting glucose and hydrogen peroxide†

Yunfan Qiao,[a] Rushi Zhao,[b] Min Zhang,*[b] Hongyang Zhang,[a] Yuerong Wang[a] and Ping Hu *[a]

In this paper, we presented a new method for constructing near-infrared fluorescence probes and their applications in detecting glucose and hydrogen peroxide (H_2O_2). We used purified (6,5) single-wall carbon nanotubes (SWCNTs) separated by a polyethylene glycol/dextran aqueous two-phase system as the basis for near-infrared probes. Different phenylboronic acids were used for non-covalent modification of SWCNTs (6,5). Glucose was detected by the specific binding of the boronic acid group with *cis*-diol. Hydrogen peroxide was detected by horseradish peroxidase (HRP) combined with phenylboronic-acid-modified SWCNTs. The results revealed that the fluorescence intensity of purified SWCNTs was significantly enhanced without other chiral nanotube interactions compared to that of the raw SWCNT material. The fluorescence responses of 3-carboxy-5-nitrophenylboronic acid-modified purified CNTs could be used to effectively measure glucose in the concentration range from 0.01 mM to 0.50 mM with an interval linear index of $R^2 = 0.996$ (LOD = 1.7 μM, S/N = 3). The detected H_2O_2 with the 3-aminobenzeneboronic acid-modified (6,5) SWCNT with HRP was in the concentration range from 5.0 μM to 40 μM with an interval linear index of $R^2 = 0.997$ (LOD = 0.85 μM, S/N = 3). Moreover, this sensor exhibited a strong anti-interference effect without biological matrix fluorescence effects above 1000 nm wavelength. Thus, the proposed novel near-infrared fluorescence probes employed for reducing the interference of the biomatrix in this region are expected to be used in subsequent biosensor investigations.

Received 9th November 2018
Accepted 21st December 2018

DOI: 10.1039/c8ra09272a

rsc.li/rsc-advances

1. Introduction

Single-wall carbon nanotubes (SWCNTs) have a stable and strong fluorescence in the near-infrared (NIR) region.[1,2] In view of this special advantage, SWCNTs have been widely used as NIR optical sensors for detecting glucose,[3] nitric oxide,[4] nitro-aromatics,[5] and proteins[6,7] by monitoring the fluorescence of SWCNTs after selective binding to the target analytes even at the single-molecule level.[8–10] The NIR fluorescence probe provides a unique advantage over conventional fluorophores, which typically bleach and fluoresce in the ultraviolet or visible region. SWCNT NIR probes can overcome the challenges encountered because biological tissues are optically transparent and have minimal auto-fluorescence in the NIR wavelengths.[11] Different chiral SWCNTs have varied absorption wavelengths,[12] which results in uncontrollable interference during the application of unsorted SWCNTs for NIR detection because of the presence of different chiral CNTs. Hence, separation and purification of chiral SWCNTs are necessary for their application to detect biomolecules.

Diabetes is a metabolic disorder syndrome, which can cause mellitus-induced heart disease, kidney failure, or blindness due to insulin deficiency and is reflected by high blood glucose concentrations.[13] Blood glucose monitoring is necessary for treatment and prevention of this disease. Enormous efforts have thus been invested to develop glucose biosensors to determine and monitor the level of glucose in the blood. These methods mainly depend on electrochemistry,[14] optical techniques,[15–17] spectroscopy,[17,18] and field-effect transistors (FETs).[19] Among them, optical techniques have been widely applied because of simple operation, quick response and low cost for further applications.[20] However, most of these optical techniques are based on visible-region fluorescence, which may lead to interference signals from the biological matrices during further applications. By contrast, the probe having stable and strong fluorescence in the NIR region can overcome this defect. This leads to an attractive approach for the study of living cells

[a]*Shanghai Key Laboratory of Functional Materials Chemistry, School of Chemistry and Molecular Engineering, East China University of Science and Technology, Shanghai 200237, China. E-mail: huping@ecust.edu.cn*

[b]*Shanghai Key Laboratory of New Drug Design, School of Pharmacy, East China University of Science and Technology, Shanghai 200237, China. E-mail: zhangm@ecust.edu.cn*

† Electronic supplementary information (ESI) available. See DOI: 10.1039/c8ra09272a

in vivo. Boronic acids are excellent molecular receptors for saccharides and glycoproteins[21,22] in electrochemical[23–25] and fluorescence[22,26–28] sensors. Boronic acids can bind to the 1,2-*cis*-diol structure of glucose and modulate the signal response of sensors. A recent report showed that novel magnetic composites functionalized by boronic acids to form sandwich-like nanostructures can be applied to determine human platelet-derived growth factor. The method could achieve a remarkable detection limit of 0.22 fM.[29] As a reactive oxygen species, hydrogen peroxide (H_2O_2) is a key analyte because of its wide applications in biology, biomedicine, food security, and environmental protection.[30–32] H_2O_2 is commonly considered as a biomarker that can reflect human health. H_2O_2 not only induces cytotoxic effects but also acts as a signal molecule that regulates different biological processes such as immune cell activation, vascular remodeling, and apoptosis. H_2O_2 plays an important regulatory role in health and disease diagnosis. Given that H_2O_2 is a byproduct of many enzymatic reactions, its concentration can be used as an indicator to track biochemical processes.[33–35] Therefore, an accurate and sensitive method must be established for detecting H_2O_2 in the cell environment.

To date, several analytical techniques have been proposed for H_2O_2 detection including spectrometry,[36] fluorometry,[37,38] chromatography,[39,40] cell imaging,[41,42] and electrochemical methods.[43,44] Among these methods, fluorometry is an H_2O_2 detection strategy characterized by simplicity, easy operation, rapid response time, high sensitivity, and excellent selectivity. Fluorometry using fluorescent nanomaterials functionalized with a natural enzyme horseradish peroxidase (HRP) was found to be an attractive method for H_2O_2 sensing.[28] However, the fluorescence in the visible region is easily disturbed by the biological matrix, which greatly restricts the potential application of this approach for *in vivo* detection.

In vivo and in-time detection of biomarkers by biosensors is the goal for bioanalysis, and the biocompatibility of CNTs is gradually being explored. For example, SWCNTs have been used *in vivo* as optical probes for plants and small animals.[45–47] In view of the lack of biological fluorescence interference in the NIR regions of SWCNTs, SWCNT-based NIR optical sensing of glucose and H_2O_2 has great potential for *in vivo* sensors. Here, we report the first application of purified single chiral SWCNTs (6,5) by aqueous two-phase extraction for preparation of NIR probes. An NIR fluorescence sensor for glucose detection was prepared by non-covalently binding phenylboronic acid to the sidewalls of SWCNTs. Then, we functionalized HRP on this sensor by utilizing HRP's *cis*-diol structure to establish a good measurement detector of H_2O_2 (Scheme 1).

2. Experimental section

2.1 Materials

Polyethylene glycol (PEG, 6 kDa) was purchased from Alfa Aesar. Dextran (DEX, 70 kDa) was purchased from TCI. Sodium dodecyl sulfate (SDS) was acquired from Sigma-Aldrich. Horseradish peroxidase was purchased from Shanghai Titan Scientific Co., Ltd. Phenylboronic acid was purchased from Aladdin. Various phenylboronic acid derivatives (3-nitrophenylboronic acid (3NPBA), 4-nitrophenylboronic acid (4NPBA), 2-carboxybenzeneboronic acid (2CPBA), 3-carboxybenzeneboronic acid (3CPBA), 4-carboxybenzeneboronic acid (4CPBA), 3-aminophenylboronic acid (3AMBA), 3-carboxy-5-fluorobenzeneboronic acid (5F3CPBA), 3-carboxy-5-nitrophenylboronic acid (5N3CPBA), 5-carboxy-2-chlorobenzene boronic acid (2Cl5CPBA) 3-amino-4-methylbenzene boronic acid (3A4MPBA), 4-carboxy-3-fluorophenylboronic acid (4C3FPBA), 9-anthraceneboronic acid (9ANBA), 9-phenanthreneboronic acid (9PHBA), 4-methyl-1-naphthaleneboronic acid (4M1NPBA)) were purchased from Aladdin. 4-Chlorophenyl boronic acid (4CYBA) and 3-acetylphenylboronic acid (3ACPBA) were purchased from Adamas-beta (chemical structures are in Table S1†). Ultrapure water (18.2 MΩ cm) was used throughout the experiment.

2.2 Instruments and characterizations

UV/Vis/NIR spectra of all SWCNT solutions were obtained by using a SHIMADZU UV-2600 scanning spectrophotometer. The NIR fluorescence of the SWCNT solutions was measured using a QM/TM fluorescence spectrometer (Photon Technology Canada Inc.). Sample excitation was from a 560 nm photodiode laser. The SWCNT dispersion was centrifuged in a GT 16-WS ultrasonication centrifuge obtained from Thermo Fisher Scientific. The samples were put in a quartz fluorescence cuvette with 10 mm optical path length. The samples were excited by light with a wavelength of 560 nm, and the emission spectrum was recorded in the range from 900 to 1300 nm.

2.3 Separation of (6,5) SWCNT

First, 1 mg of SWCNT raw material was dispersed in 1 mL of 2 wt% sodium deoxycholate (SDC) solution. The samples were sonicated in an ice water bath for 1 h at 225 W and then ultracentrifuged for 1 h at 18*g* and 19 °C. After centrifugation, the supernatant was collected to obtain a uniformly dispersed SWCNTs–SDC dispersion. Then, 20 mL of 15 wt% PEG and 20 mL of 15 wt% DEX were mixed in a 50 mL centrifuge tube. After reaching equilibrium, the upper phase and the lower phase were collected for further separation.

A volume of 10 μL of the SWCNTs–SDC dispersion and 18 μL of 10 wt% SDS solution were added to 250 μL of 15 wt% PEG and 250 μL of 15 wt% DEX ATP system and then centrifuged for 30 s at 5000 rpm and room temperature after mixing. Then, 4 μL of $MgCl_2$ (ionic strength, I = 0.5 mol kg^{-1}) was added and centrifuged under the same conditions. The bottom (B) phase was collected, and 250 μL of the new upper phase was added to B to obtain a new ATP system. The amounts of 10 wt% SDS, 2 wt% SDC, and 0.05 M HCl that were added to the aqueous two-phase system were adjusted to make the upper phase olive in color. The bottom phase BB was collected, and 250 μL of the new upper phase was added to BB to obtain a new ATP system. The amounts of 10 wt% SDS, 2 wt% SDC, and 0.05 M HCl that were added to the aqueous two-phase system were adjusted to make the top (T) phase purple in color. The top phase BBT was the purified SWCNT (6,5) sample. The purified samples were heated and cleaned to remove the salts and the acids during

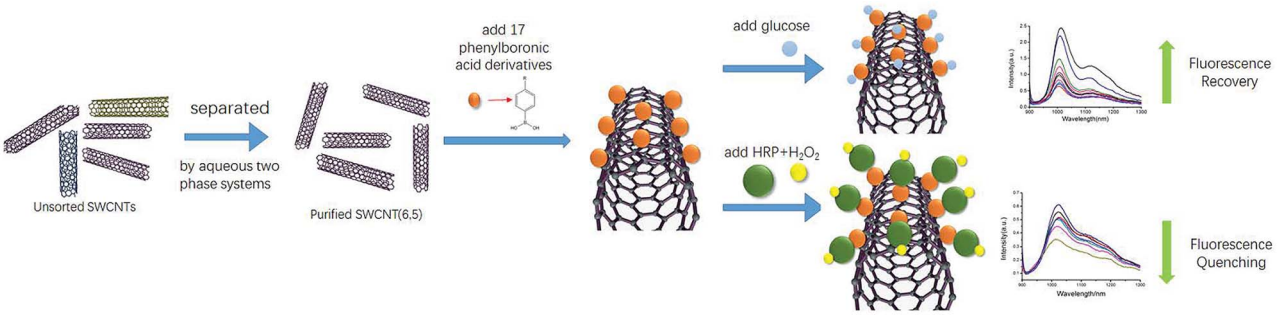

Scheme 1 Diagram of glucose and H_2O_2 detecting complex. The phenylboronic acid derivative lies on the sidewalls of the nanotube and initially quenches SWCNT. In the presence of diols, the hydroxyl of the boron can bind with 1,2-diols to form diol–phenylboronic complexes with five-membered rings, which changes the photoluminescence intensity of SWCNT. Besides, HRP can specifically bind H_2O_2, which can also change the fluorescence of the functionalized SWCNT. The change in the concentration of H_2O_2 can be reflected in the change in fluorescence by utilizing this feature.

separation. Then, the samples were re-dispersed in 1% SDS concentration by the same method used for unsorted SWCNTs. The purified CNTs were characterized by UV/Vis/NIR spectra through the purity of the sample based on the chiral carbon tube specific E_{11} and E_{22} peaks.

2.4 Method of phenylboronic acid-functionalized SWCNT sensor for glucose detection

All phenylboronic acids were dissolved in DMSO at 0.1 M concentration. Ten μL of phenylboronic acid solution was added to 190 μL of the purified SWCNT solution. The concentration of the purified SWCNTs (6,5) was 0.06 mg mL^{-1} after calculation (Fig. S1†). The mixture solution was incubated for 30 min at room temperature.

Ten μL of the glucose solution dissolved in 1 M PBS buffer solution (pH 7.4) was added to 190 μL of the prepared SWCNT solution. A total of 17 kinds of incubated phenylboronic acid-functionalized SWCNT solutions were needed to make the final glucose concentration to 0.2 mM. After quick mixing, the fluorescence spectra of the mixture solution were consistently monitored at 30 min intervals at room temperature.

2.5 Method of phenylboronic acid-functionalized SWCNT sensor for H_2O_2 detection

A PBA-HRP-SWCNT sensing system was established using the following procedures. Phenylboronic acids were dissolved in DMSO at 0.1 M concentration; 10 μL of the phenylboronic acid solution was added to 190 μL of the prepared SWCNT solution. The mixture solution was incubated for 30 min at room temperature. Then, 10 μL of HRP solution (1 mM) dissolved in 1 M PBS buffer solution (pH 7.4) was added to 190 μL of the incubated phenylboronic acid-functionalized SWCNT solution. The mixture solution was incubated for 10 min at room temperature.

Ten μL of H_2O_2 solution dissolved in 1 M PBS buffer solution (pH 7.4) was added to 190 μL of the HRP-incubated phenylboronic acid-functionalized SWCNT solution. After quick mixing, the fluorescence spectra of the mixture solution were consistently monitored at 30 min intervals at room temperature.

2.6 Fluorescence assay for glucose

A fluorescence glucose assay was performed using the following procedures. Different amounts of glucose were dissolved in 1 M PBS buffer solution (pH 7.4). We chose 5-nitro-3-carboxyphenyl boronic acid-functionalized SWCNTs as the glucose sensor. The method of glucose detection was the same as that described in Section 2.4. A fluorescence assay was conducted on potential interfering substances under the same conditions.

2.7 Fluorescence assay for H_2O_2

Different amounts of H_2O_2 were dissolved in 1 M PBS buffer solution (pH 7.4). We chose 3-aminophenylboronic acid-functionalized SWCNTs as the H_2O_2 sensor. The method of H_2O_2 detection was the same as that described in Section 2.5. We used HeLa cells in real sample detection of H_2O_2. The HeLa cells were cultured in a culture vessel containing 15 mL of DMEM medium with 10% fetal bovine serum and 1% penicillin/streptomycin. The vessel was placed in a humid incubator under an atmosphere consisting of 95% air and 5% CO_2 at 37 °C. When the cells reached confluence, the number of HeLa cells was counted using microscopy and calculated as 3.2×10^5. All cells were collected through centrifugation (1000 rpm, 5 min) and dispersed in 4 mL of PBS solution for the subsequent fluorescence test. Ten μL of pretreated cell solution samples was added to 190 μL of the incubated HRP phenylboronic acid-functionalized SWCNT (6,5) solution and reacted for 30 min. Then, the fluorescence intensity was measured.

3. Results and discussion

3.1 Comparison between unsorted CNTs and purified SWCNTs (6,5)

The UV-VIS-NIR spectra of unsorted SWCNTs and purified SWCNTs (6,5) are shown in Fig. 1. When SWCNTs are sorted by the aqueous two-phase system, other chiral SWCNTs except for (6,5) are nearly excluded in the UV-VIS-NIR spectrum. In the UV

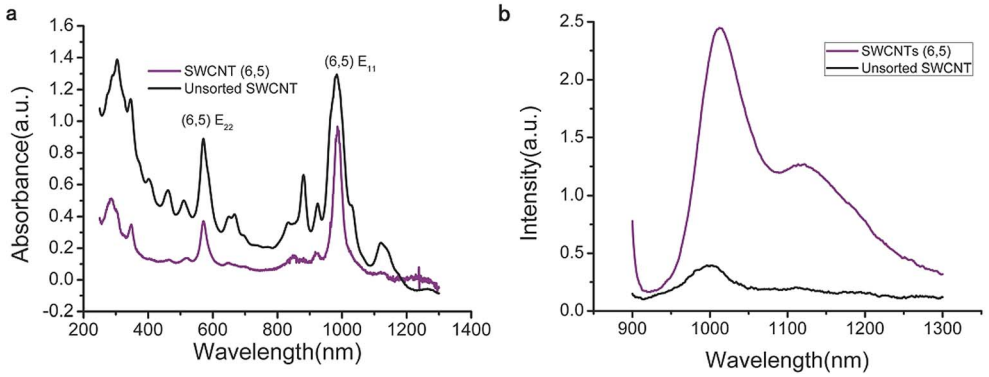

Fig. 1 UV-VIS-NIR spectrum (a) and fluorescence spectrum (b) that compare the purified SWCNTs (purple) and unsorted SWCNTs (black). In the fluorescence spectrum, the concentration of purified SWCNTs (6,5) is 0.06 mg mL^{-1} after calculation according to absorbance value (Fig. S1†), and the concentration of unsorted SWCNTs is 0.33 mg mL^{-1} after calculation according to absorbance value (dispersed in 1% SDS solution). Excitation at 560 nm.

absorption spectrum, except for the characteristic E_{11} (at 560 nm) and E_{22} peaks (at 990 nm) of SWCNTs (6,5), the absorption peaks of other chiral carbon nanotubes nearly disappear. At 560 nm excitation, the emission spectra of the two fluorescence patterns differed greatly. Purified SWCNTs were superior to unsorted CNTs. The possible reason is that other chiral carbon tubes significantly affected the quenching of SWCNTs (6,5). After separation of CNTs, the NIR fluorescence intensity was significantly enhanced; hence, we chose purified SWCNTs for fabricating the probes.

Fig. 2 shows the fluorescence spectra of CNTs combined with phenylboronic acid derivatives. The purified and unsorted CNTs exhibited significantly varied fluorescence intensities. For example, for 5-nitro-3-carboxyphenylboronic acid-functionalized two kinds of CNTs, although the phenylboronic acid derivatives exerted a quenching effect on both CNTs according to fluorescence spectroscopy, the fluorescence intensity recovery greatly varied after glucose was added. In view of the sensitivity and intensity of the fluorescence signal, the purified CNTs offered a great advantage. The possible reason is that for unsorted CNTs, other chiral carbon nanotubes could quench SWCNTs (6,5), and this effect is markedly clear such that the fluorescence intensity of the carbon nanotubes varies greatly. Other chiral CNTs not only quenched the fluorescence of the carbon nanotubes but also combined with phenylboronic acid derivatives, thereby further reducing the sensitivity and stability of the carbon nanotubes as sensors. This phenomenon is the main reason for the use of purified CNTs in the following experiment. The effects of other chiral carbon nanotubes were reduced because of the separation of the carbon nanotubes, and the fluorescence performance of the sensors greatly improved.

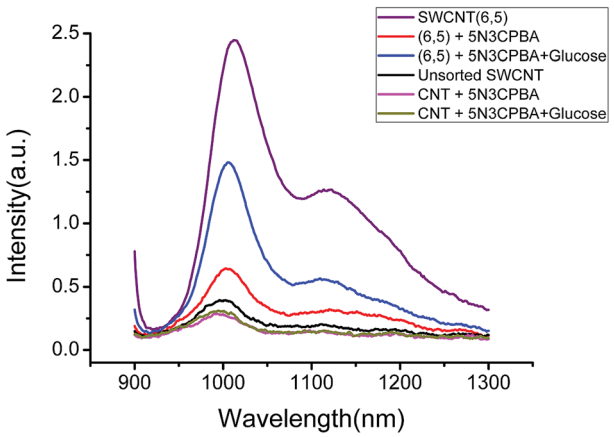

Fig. 2 Representative fluorescence spectra that compare the original spectra of the two kinds of SWCNTs (purple and black), the spectrum after adding 5-nitro-3-carboxyphenylboronic acid to the two SWCNT solutions (red and magenta), and the spectrum after adding glucose to the two PBA-SWCNT complex solutions (blue and dark yellow). Excitation at 560 nm.

3.2 Screening of phenylboronic acid derivatives

Phenylboronic acids can reversibly form stable phenylboronic complexes with *cis*-diols, which allow the detection of a wide range of saccharide markers. A generally accepted hypothesis is that aromatic boronic acids are conjugated on the surface of SWNTs through π–π interactions between the hydrophobic sidewall of SWCNTs and the aromatic moiety of boronic acids, which affects the fluorescence intensity of SWCNTs. The 1,2-*cis*-diol structure of glucose can combine with phenylboronic acids and modulate the fluorescence intensity of SWNTs when glucose is added. Strano and coworkers[48] used different phenylboronic acids combined with CNTs wrapped with different surfactants to detect saccharides. Although they performed excellent screening on the phenylboronic acid derivative-modified carbon tubes, the carbon tubes were not completely purified and the fluorescence was not improved. No study has considered the differences in the binding ability of phenylboronic acid and the fluorescence effects of purified CNTs. In this study, we used purified SWCNTs (6,5) for detecting glucose. As shown in Fig. 3, the CNTs were quenched in the NIR region after their sidewalls combined with phenylboronic acid derivatives through π–π stacking interactions.

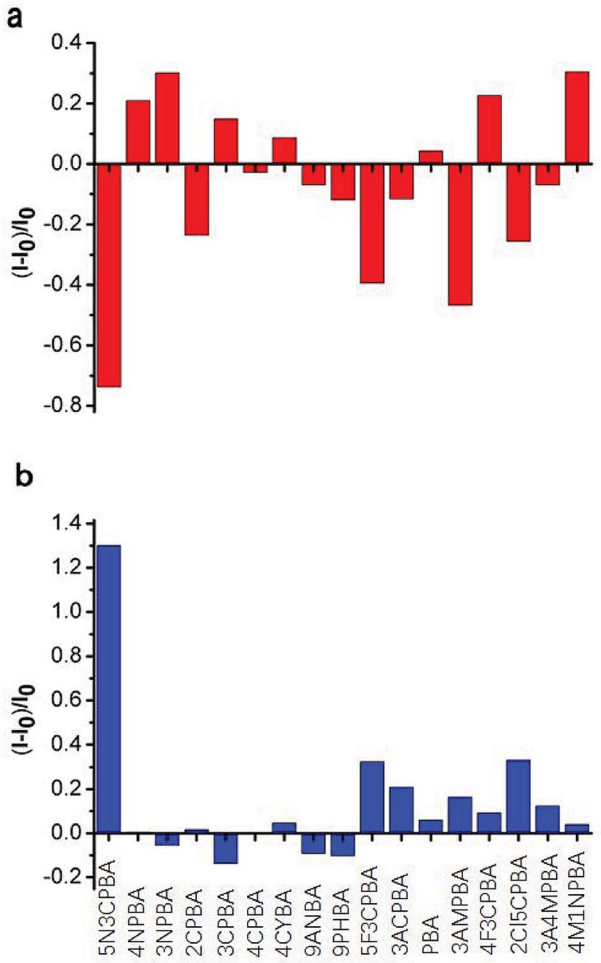

Fig. 3 Screening of the reactivity of SWCNTs (6,5) with 17 phenylboronic acid derivatives and the fluorescence response of the 17 phenylboronic acid-functionalized purified SWCNTs (6,5) to glucose. (a) Fluorescence intensity change (red) of purified SWCNTs (6,5) after the addition of 17 different phenylboronic acid derivatives. (b) Fluorescence intensity change (blue) of purified SWCNTs (6,5) after the subsequent addition of 0.2 mM glucose to the 17 phenylboronic acid derivative-functionalized purified SWCNT (6,5) complexes shown in (a). Excitation at 560 nm and emission wavelength at 1010 nm.

Fig. 3a shows the fluorescence response to the addition of various phenylboronic acid derivatives calculated by Fig. S2.† Ten phenylboronic acids quenched the fluorescence intensity of purified CNTs. Among them, the phenylboronic acid derivatives double-substituted on the phenyl ring (except 4-fluoro-3-carboxyphenylboronic acid) induced a quenching effect on SWCNTs (6,5). For mono-substituted phenylboronic acid derivatives, nitro-substitution increased the fluorescence of SWCNTs (6,5). Amino-substitution at the third position on the phenyl ring also showed a good quenching effect. One possible explanation is that different substituents of phenylboronic acid derivatives affected the probability density of the electrons on the phenyl ring, which presented a different effect through π–π stacking interactions on the binding of empty orbitals in the sidewalls of SWCNTs (6,5). The binding ability and binding mechanism of different phenylboronic acid derivatives to carbon tubes determined their influence on the fluorescence of SWCNTs (6,5).

With regard to the response to glucose addition, the phenylboronic acid derivative on the sidewall of the carbon tube bound to the *cis*-diol structure of glucose after glucose was added to the phenylboronic acid-modified CNTs, resulting in fluorescence recovery of CNTs. In these phenylboronic acid derivatives, 5-nitro-3-carboxyphenylboronic acid-functionalized SWCNTs (6,5) displayed good fluorescence recovery, as shown in Fig. 2b. Thus, we chose this sample for linear analysis and selectivity experiment for the sensor.

3.3 Sensitivity and kinetics of the fluorescent SWCNT glucose sensors

We measured the linear response range of the phenylboronic acid derivatives combined with the SWCNT sensing system. As shown in Fig. 4, the fluorescence intensities of 5-nitro-3-carboxy phenylboronic acid-functionalized SWCNTs (6,5) were highly sensitive to glucose, and they increased as the analyte concentration increased. We used the emission peak wavelength at 1010 nm of (6,5) to calculate the intensity change (I–I_0) and establish the calibration curve (Fig. 4b).

The relationship between the analyte and the available docking sites for glucose can be described as follows:

$$\mathrm{PBASWCNT + GLU} \rightleftharpoons \mathrm{GLUPBASWCNT} \tag{1}$$

The calibration curve can be described by a kinetic adsorption model, in which G is the analyte glucose, S is an available recognition site on the SWCNT sensor, and SG is the product of this reaction. The equilibrium for this reaction can be modeled as an instantaneous reaction and described by the following equilibrium constant:

$$K = \frac{[\mathrm{SG}]}{[\mathrm{S}][\mathrm{G}]} \tag{2}$$

S_{tot} denotes the total recognition sites of the free and occupied sites.

$$S_{\mathrm{tot}} = [\mathrm{SG}] + [\mathrm{S}] \tag{3}$$

We can use eqn (2) and (3) to derive the following expression for S_{tot} in terms of the glucose concentration [G]:

$$\begin{aligned} S_{\mathrm{tot}} &= [\mathrm{SG}] + [\mathrm{S}] \\ &= [\mathrm{SG}] + \frac{[\mathrm{SG}]}{K[\mathrm{G}]} \\ &= [\mathrm{SG}]\left(1 + \frac{1}{K[\mathrm{G}]}\right) \\ &= [\mathrm{SG}]\left(\frac{K[\mathrm{G}] + 1}{K[\mathrm{G}]}\right) \end{aligned} \tag{4}$$

If we assume that the sensor response (*i.e.*, the normalized intensity change) is proportional to the $\frac{[\mathrm{SG}]}{S_{\mathrm{tot}}}$ ratio, we find that

$$\frac{I - I_0}{I_0} = \alpha\frac{[\mathrm{SG}]}{S_{\mathrm{tot}}} + B = \alpha\frac{K[\mathrm{G}]}{K[\mathrm{G}] + 1} + B \tag{5}$$

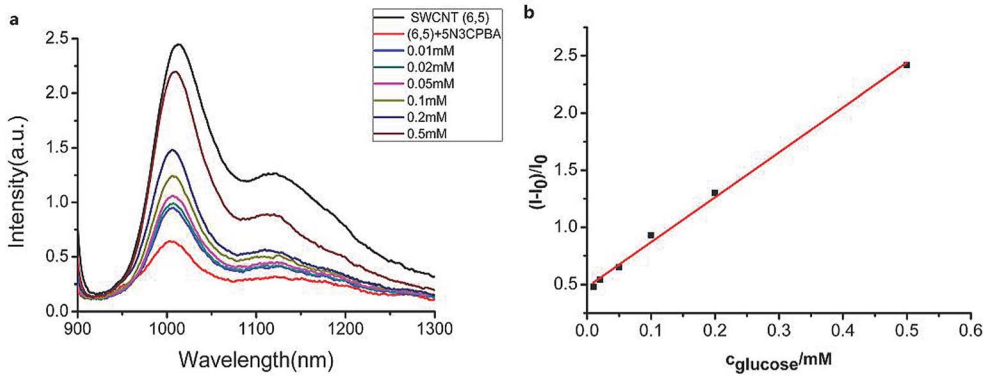

Fig. 4 (a) Fluorescence spectra of the 5-nitro-3-carboxyphenylboronic acid-functionalized SWCNTs (6,5) at various glucose concentrations. (b) Linear plots of the reduced intensity of the SWCNT (6,5) fluorescence as linear relationship of glucose concentration, $R^2 = 0.996$. I_0 and I are the corresponding fluorescence intensities of SWCNTs in the absence and presence of the analytes. Excitation at 560 nm and emission wavelength at 1010 nm.

where B is the background, and α is the proportionality factor. Given that the curve is linear in the glucose concentration range from 10 μM to 500 μM, $K[G] + 1$ can be approximated as 1. Thus, eqn (5) can be approximated as

$$\frac{I - I_0}{I_0} = \alpha K[G] + B \quad (6)$$

Fitting the curve in Fig. 4b indicated that a good linear relationship ($R^2 = 0.996$) existed between the fluorescence intensities and the glucose concentrations in the range from 10 μM to 500 μM as $\alpha K = 3.93$ and $B = 0.47$ with 1.7 μM detection limit (S/N = 3). This value was calculated by adding the sensor response for the addition of only PBS solution to thrice the standard deviation and then using the fit to eqn (6) to calculate the concentration.

3.4 Selectivity of the fluorescent SWCNT glucose sensors

Selectivity is a key parameter in assessing the performance of fluorescent chemosensors and is particularly important in the blood serum samples of biological samples with complex matrices. We examined the fluorescence responses of SWCNTs toward potential interfering substances coexisting in various amino acids, inorganic salts, and uric acid. As shown in Fig. 5, these substances only minimally affected (either by fluorescence quenching or enhancement) the SWCNT fluorescence.

3.5 Real sample detection of glucose

To investigate the potential practical applications of this method, we detected glucose in human serum. Pretreated serum solution samples (10 μL) were added to 190 μL of the prepared SWCNT (6,5) sensor system and reacted for 30 min. Then, the fluorescence intensity was measured. Table 1 shows the glucose concentrations obtained by our proposed method.

3.6 Determination of H_2O_2 by phenylboronic acid derivative-modified SWCNT (6,5) probe

As a glycoprotein, HRP has been proven to contain 21.8% carbohydrates,[49] due to which it can be combined with boronic acid groups. Due to the specific binding of HRP to H_2O_2, we prepared a PBA-HRP-SWCNT sensor for H_2O_2 detection. On the basis of the preliminary screening of phenylboronic acid derivatives, five phenylboronic acid derivatives were selected for further analysis of H_2O_2 detection. Considering the fluorescence quenching of the purified SWCNTs by phenylboronic acid, as shown in Fig. 2, HRP did not significantly affect the 3AMBA-modified CNT fluorescence, whereas the fluorescence changed significantly after the addition of H_2O_2, as shown in Fig. 6. The variation in NIR fluorescence of SWCNTs was due to electron transfer when H_2O_2 was combined with PBA-HRP-

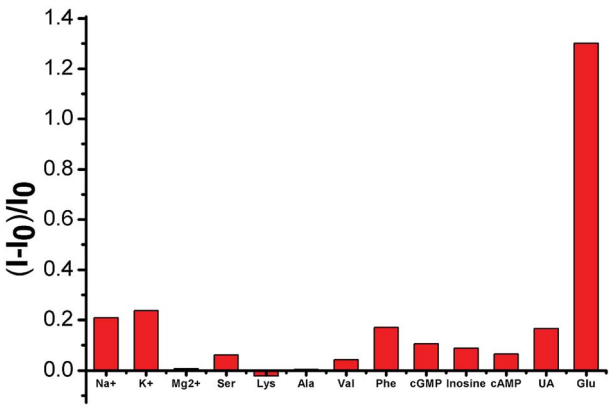

Fig. 5 SWCNT-based system for various potential interfering substances. The concentrations of various inorganic salts (from left to right) are 0.16, 5.6, and 0.04 mM. The concentrations of various amino acids (from left to right) are 6, 6, 14, 8, and 30 μM. The concentrations of various nucleosides (from left to right) are 0.2, 200, and 0.1 nM. The concentrations of uric acid and glucose are 12 and 200 μM, respectively. The concentrations of potential interfering substances correspond to 25-fold dilution of those in serum considering the proper concentration of glucose detected by this sensor.

Table 1 Glucose detection in human serum

Samples	Content glucose/μM	Added glucose/μM	Found glucose/μM	Recovery (%)	RSD (%)
1	69	50	123	108	3.6
2	69	100	165	96	3.6
3	69	200	296	113	3.1

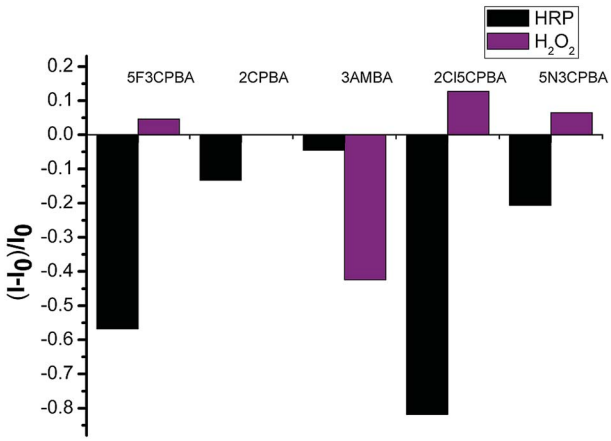

Fig. 6 SWCNT fluorescence responses of five kinds of phenylboronic acids to HRP modification and subsequent detection of H_2O_2. The black column shows the effect of HRP on the fluorescence of five phenylboronic acid-modified SWCNTs (6,5). The purple column shows the effect of H_2O_2 on the fluorescence of five PBA-HRP-modified SWCNTs (6,5).

SWCNT. The combination of HRP and different derivatives of PBA-modified SWCNTs showed significant impact on the fluorescence intensity of SWCNTs. We assumed that the intensity change was due to the structural differences in the PBA derivatives. Although the four other phenylboronic acid derivative-modified SWCNTs (6,5) presented stronger fluorescence changes than 3AMBA after HRP addition, their fluorescence response to the analyte did not reach the level of signal variation.

To utilize phenylboronic acid-functionalized purified CNTs, HRP was combined with the probe to detect H_2O_2. The purified CNTs showed a good fluorescence signal and sensitivity to hydrogen peroxide (Fig. 7a). The unsorted CNTs exhibited nearly no response to hydrogen peroxide. The possible reason is that the ability of other chiral CNTs to bind PBA-HRP was stronger than that of SWCNTs (6,5), leading to the lack of quenching of the fluorescence signal at this wavelength after the addition of hydrogen peroxide. Another possible reason is that the signal variation was too small to recognize its change. In a previous research, it was reported that H_2O_2 affected the optical properties of CNTs due to its oxidation effect on SWCNTs.[10] In this paper, the introduction of H_2O_2 to PBA-SWCNT did not have significant fluorescence changes, as shown in Fig. 7b. We assumed that the boronic acid group that modified the SWCNT sidewall hindered the redox reaction. Meanwhile, boronic acid might also inhibit the dissolved oxygen in water from having an oxidation effect on SWCNTs. With the aid of HRP, H_2O_2 could be recognized by the sensor.

3.7 Sensitivity of the fluorescent SWCNT H_2O_2 sensors

The linear response range of the PBA-HRP-CNT sensing system was measured with the purified CNT probe. As shown in Fig. 8, a good linear relationship $\left(\frac{I-I_0}{I_0} = 0.0081C_{(H_2O_2)} + 0.1007,\ R^2 = 0.997\right)$ existed between the fluorescence intensities and the concentrations of H_2O_2 in the range from 5 μM to 40 μM with detection limit of 0.85 μM (S/N = 3). The fluorescence intensity was quenched with increasing H_2O_2 concentration. As we assumed, H_2O_2

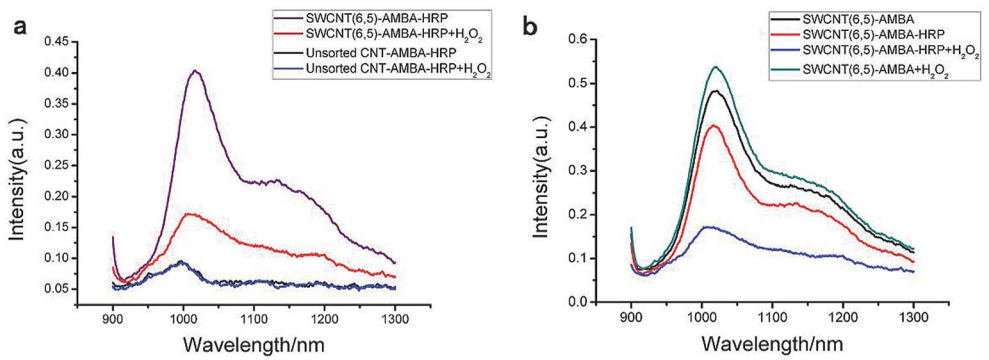

Fig. 7 (a) Representative fluorescence spectra that compare two kinds of SWCNTs detecting H_2O_2, the spectrum after adding horseradish peroxidase to two SWCNT solutions (purple and black), and the spectrum after adding 40 μM H_2O_2 to the two 3AMBA-HRP-SWCNT complex solutions (red and blue). (b) Fluorescence spectra of SWCNTs (6,5) mixed with 3AMBA, 3AMBA + HRP, 3AMBA + HRP + H_2O_2, and 3AMBA + H_2O_2. The concentration of H_2O_2 was 40 μM.

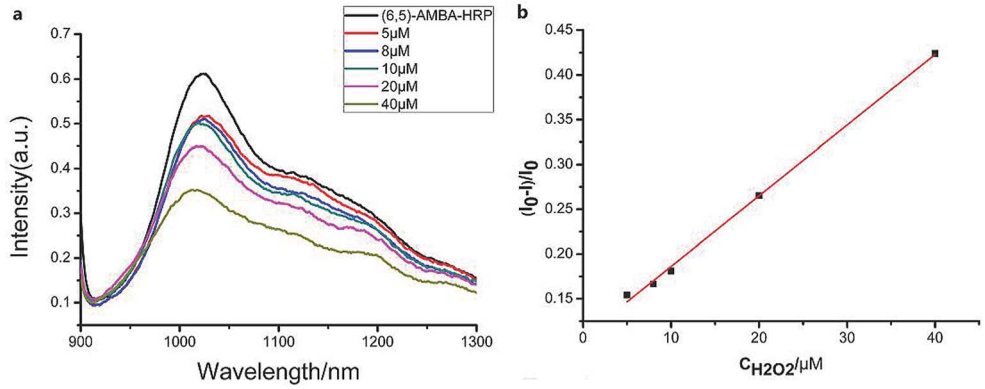

Fig. 8 (a) Fluorescence spectra of the 3AMBA-HRP-functionalized SWCNTs (6,5) at various H_2O_2 concentrations. (b) Linear plots of the reduced intensity of the SWCNT (6,5) fluorescence as linear relationship of H_2O_2 concentration, $R^2 = 0.997$. I_0 and I are the fluorescence intensities of the SWCNTs in the absence and presence of analytes, respectively.

Table 2 Comparison of the nanomaterial-based sensors for the detection of H_2O_2

Sensors	Methods	Detection limit/μM	Linear range/μM	Ref.
HRP-BMIM·BF_4/SWCNTs/CFUME	Electrochemical	0.13	0.49–10.2	50
Nitrogen-doped CNTs	Electrochemical	0.5	Not reported	51
AuNPs/4-CA	SERS	0.08	0.1–20	52
HTP-AuNCs	SERS	0.07	0.1–2.53	36
dLys-AgNCs	Fluorescence	0.2	0.8–200	53
HRP-MWCNT	Fluorescence	1.2	Not reported	28
dsDNA-SWCNT	NIR absorption	Not reported	29–5900	54
3AMBA-HRP-SWCNT	NIR fluorescence	0.85	5–40	This work

might change the conformation/structure of HRP and PBA-HRP-SWCNT. The change in the surrounding environment of SWCNTs may result in fluorescence quenching. The high concentration of hydrogen peroxide could lead to complete fluorescence quenching of CNTs, which is the main constraint of this sensor. Various H_2O_2 determination results based on nanomaterial biosensors are listed in Table 2. It demonstrates that the 3AMBA-HRP-SWCNT sensor has an advantage for H_2O_2 determination. It was suggested that HRP in the functionalized SWCNTs provided an active site that was more conducive to the detection of H_2O_2. Additionally, the fluorescence emission affected by this combination in the NIR region exhibited a large Stokes shift. This advantage allowed the sensor to be less affected by interference in real samples, suggesting that the sensor could be applied for biosensing.

3.8 Real sample detection of H_2O_2

Table 3 shows the H_2O_2 concentrations obtained by our proposed method. The concentration of H_2O_2 in HeLa cells was determined to be lower than the detection limit of this method. Thus, the feasibility of the method was verified by the cell culture solution after H_2O_2 addition. The result shows that the method proposed in this study has good performance with respect to H_2O_2 detection in real samples because of small interference in the NIR fluorescence region, suggesting that this method is promising for glucose determination in medical diagnosis and biological analysis.

Table 3 H_2O_2 detection in HeLa cell suspension

Samples	Added H_2O_2/μM	Found H_2O_2/μM	Recovery (%)	RSD (%)
1	10	11.8	118	9.9
2	20	20.4	102	4.7
3	30	28.2	94.0	0.9

4. Conclusion

In conclusion, we demonstrated that purified SWCNTs (6,5) can be used as a raw material of potential sensors and probes in the NIR region. The separation of carbon tubes greatly enhanced the fluorescence signal of CNTs of the same concentration. In addition, we examined the effect of 17 phenylboronic acid derivatives on the fluorescence of SWCNTs (6,5) in the NIR region. The possible reason for the change in the carbon tube fluorescence is that different substituents of the phenylboronic acid derivatives affected the probability density of the electrons on the phenyl ring, which had different combinations of SWCNT (6,5) sidewalls. Given the absence of the fluorescence interference of other chiral carbon tubes, we used sugar and hydrogen peroxide as examples to demonstrate the excellent role of non-covalently modified purified CNTs in the field of detection. In the experiments, we chose 5-nitro-3-carboxyphenylboronic acid-functionalized SWCNTs (6,5) as the glucose sensor, which exhibited good ability for

concentration measurements and anti-interference in complex environments. Moreover, we briefly studied the fluorescence response of phenylboronic acid derivatives combined with SWCNTs (6,5) and enzymes, and we selected 3AMBA-HRP-functionalized SWCNTs (6,5) as the sensor for detecting hydrogen peroxide. Given that biological tissues are optically transparent and minimally auto-fluorescent in the NIR wavelengths, this study provides a new stable and robust NIR fluorescence sensor material for subsequent biosensor investigations.

Conflicts of interest

There are no conflicts to declare.

Acknowledgements

We thank Dr Geyou Ao for her critical comments on the manuscript. This research was financially supported by the National Natural Science Foundation of China (No. 81573397) and Shanghai Natural Science Foundation (No. 15ZR1409400).

References

1 M. J. O'Connell, S. M. Bachilo, C. B. Huffman, V. C. Moore, M. S. Strano, E. H. Haroz, K. L. Rialon, P. J. Boul, W. H. Noon, C. Kittrell, J. P. Ma, R. H. Hauge, R. B. Weisman and R. E. Smalley, *Science*, 2002, **297**, 593–596.
2 S. M. Bachilo, M. S. Strano, C. Kittrell, R. H. Hauge, R. E. Smalley and R. B. Weisman, *Science*, 2002, **298**, 2361–2366.
3 H. Yoon, J. H. Ahn, P. W. Barone, K. Yum, R. Sharma, A. A. Boghossian, J. H. Han and M. S. Strano, *Angew. Chem., Int. Ed.*, 2011, **50**, 1828–1831.
4 J. H. Kim, D. A. Heller, H. Jin, P. W. Barone, C. Song, J. Zhang, L. J. Trudel, G. N. Wogan, S. R. Tannenbaum and M. S. Strano, *Nat. Chem.*, 2009, **1**, 473–481.
5 D. A. Heller, G. W. Pratt, J. Zhang, N. Nair, A. J. Hansborough, A. A. Boghossian, N. F. Reuel, P. W. Barone and M. S. Strano, *Proc. Natl. Acad. Sci. U.S.A.*, 2011, **108**, 8544–8549.
6 B. C. Satishkumar, L. O. Brown, Y. Gao, C.-C. Wang, H. L. Wang and S. K. Doorn, *Nat. Nanotechnol.*, 2007, **2**, 560–564.
7 J. H. Ahn, J. H. Kim, N. F. Reuel, P. W. Barone, A. A. Boghossian, J. Zhang, H. Yoon, A. C. Chang, A. J. Hilmer and M. S. Strano, *Nano Lett.*, 2011, **11**, 2743–2752.
8 L. Cognet, D. A. Tsyboulski, J.-D. R. Rocha, C. D. Doyle, J. M. Tour and R. B. Weisman, *Science*, 2007, **316**, 1465–1468.
9 H. Jin, D. A. Heller, J. H. Kim and M. S. Strano, *Nano Lett.*, 2008, **8**, 4299–4304.
10 D. A. Heller, H. Jin, B. M. Martinez, D. Patel, B. M. Miller, T. K. Yeung, P. V. Jena, C. Hobartner, T. Ha, S. K. Silverman and M. S. Strano, *Nat. Nanotechnol.*, 2009, **4**, 114–120.
11 D. A. Heller, S. Baik, T. E. Eurell and M. S. Strano, *Adv. Mater.*, 2005, **17**, 2793–2799.
12 R. B. Weisman and S. M. Bachilo, *Nano Lett.*, 2003, **3**, 1235–1238.
13 C. Chen, Q. Xie, D. Yang, H. Xiao, Y. Fu, Y. Tan and S. Yao, *RSC Adv.*, 2013, **3**, 4473–4491.
14 Y. Zhang, Y. Liu, L. Su, Z. Zhang, D. Huo, C. Hou and Y. Lei, *Sens. Actuators, B*, 2014, **191**, 86–93.
15 N. Lu, M. Zhang, L. Ding, J. Zheng, C. Zeng, Y. Wen, G. Liu, A. Aldalbahi, J. Shi, S. Song, X. Zuo and L. Wang, *Nanoscale*, 2017, **9**, 4508–4515.
16 H. Sun, Y. Zhou, J. Ren and X. Qu, *Angew. Chem., Int. Ed.*, 2018, **57**, 9224–9237.
17 J. J. Xu, W. W. Zhao, S. Song, C. Fan and H. Y. Chen, *Chem. Soc. Rev.*, 2014, **43**, 1601–1611.
18 J. Yadav, A. Rani, V. Singh and B. M. Murari, *Biomed. Signal Process. Control*, 2015, **18**, 214–227.
19 K. Besteman, J. O. Lee, F. G. Wiertz, H. A. Heering and C. Dekker, *Nano Lett.*, 2003, **3**, 727–730.
20 M. S. Steiner, A. Duerkop and O. S. Wolfbeis, *Chem. Soc. Rev.*, 2011, **40**, 4805–4839.
21 T. D. James, K. R. A. S. Sandanayake and S. Shinkai, *Angew. Chem., Int. Ed. Engl.*, 1996, **35**, 1910–1922.
22 H. S. Mader and O. S. Wolfbeis, *Microchim. Acta*, 2008, **162**, 1–34.
23 E. Shoji and M. S. Freund, *J. Am. Chem. Soc.*, 2002, **124**, 12486–12493.
24 S. Takahashi and J. I. Anzai, *Langmuir*, 2005, **21**, 5102–5107.
25 A. Ori and S. Shinkai, *J. Chem. Soc., Chem. Commun.*, 1995, 1771–1772.
26 T. D. James, K. R. A. S. Sandanayake and S. Shinkai, *Nature*, 1995, **374**, 345–347.
27 H. Fang, G. Kaur and B. Wang, *J. Fluoresc.*, 2004, **14**, 481–489.
28 M. Magyar, K. Hajdu, T. Szabó, B. Endrődi, K. Hernádi, E. Horváth, A. Magrez, L. Forró, C. Visy and L. Nagy, *Phys. Status Solidi B*, 2013, **250**, 2559–2563.
29 J. Zheng, M. Zhang, X. Guo, J. Wang and J. Xu, *Sens. Actuators, B*, 2017, **250**, 8–16.
30 S. K. Yoo, T. W. Starnes, Q. Deng and A. Huttenlocher, *Nature*, 2011, **480**, 109–112.
31 G. J. DeYulia, J. M. Cárcamo, O. Bórquez-Ojeda, C. C. Shelton and D. W. Golde, *Proc. Natl. Acad. Sci. U.S.A.*, 2005, **102**, 5044–5049.
32 E. Nossol and A. J. G. Zarbin, *Adv. Funct. Mater.*, 2009, **19**, 3980–3986.
33 E. W. Miller, A. E. Albers, A. Pralle, E. Y. Isacoff and C. J. Chang, *J. Am. Chem. Soc.*, 2005, **127**, 16652–16659.
34 S. G. Rhee, *Science*, 2006, **312**, 1882–1883.
35 M. Capasso, M. K. Bhamrah, T. Henley, R. S. Boyd, C. Langlais, K. Cain, D. Dinsdale, K. Pulford, M. Khan, B. Musset, V. V. Cherny, D. Morgan, R. D. Gascoyne, E. Vigorito, T. E. DeCoursey, I. C. M. MacLennan and M. J. S. Dyer, *Nat. Immunol.*, 2010, **11**, 265–272.
36 X. Gu, H. Wang, Z. D. Schultz and J. P. Camden, *Anal. Chem.*, 2016, **88**, 7191–7197.
37 M. Ren, B. Deng, J. Y. Wang, X. Kong, Z. R. Liu, K. Zhou, L. He and W. Lin, *Biosens. Bioelectron.*, 2016, **79**, 237–243.
38 F. Wen, Y. Dong, L. Feng, S. Wang, S. Zhang and X. Zhang, *Anal. Chem.*, 2011, **83**, 1193–1196.

39 M. Song, J. Wang, B. Chen and L. Wang, *Anal. Chem.*, 2017, **89**, 11537–11544.
40 H. Yue, X. Bu, M. H. Huang, J. Young and T. Raglione, *Int. J. Pharm.*, 2009, **375**, 33–40.
41 D. Srikun, A. E. Albers, C. I. Nam, A. T. Iavaron and C. J. Chang, *J. Am. Chem. Soc.*, 2010, **132**, 4455–4465.
42 M. Abdesselem, R. Ramodiharilafy, L. Devys, T. Gacoin, A. Alexandrou and C. I. Bouzigues, *Nanoscale*, 2017, **9**, 656–665.
43 M. Zhang, J. Zheng, J. Wang, J. Xu, T. Hayat and N. S. Alharbi, *Sens. Actuators, B*, 2019, **282**, 85–95.
44 Y. Zhang, X. Bai, X. Wang, K. K. Shiu, Y. Zhu and H. Jiang, *Anal. Chem.*, 2014, **86**, 9459–9465.
45 N. M. Iverson, P. W. Barone, M. Shandell, L. J. Trudel, S. Sen, F. Sen, V. Ivanov, E. Atolia, E. Farias, T. P. McNicholas, N. Reuel, N. M. Parry, G. N. Wogan and M. S. Strano, *Nat. Nanotechnol.*, 2013, **8**, 873–880.
46 D. Ghosh, A. F. Bagley, Y. J. Na, M. J. Birrer, S. N. Bhatia and A. M. Belcher, *Proc. Natl. Acad. Sci. U. S. A.*, 2014, **111**, 13948–13953.
47 J. Pan, F. Li and J. H. Choi, *J. Mater. Chem. B*, 2017, **5**, 6511–6522.
48 K. Yum, J. H. Ahn, T. P. McNicholas, P. W. Barone, B. Mu, J. H. Kim, R. M. Jain and M. S. Strano, *ACS Nano*, 2011, **6**, 819–830.
49 B. Y. Yang, J. S. Gray and R. Montgomery, *Carbohydr. Res.*, 1996, **287**, 203–212.
50 Q. Q. Ren, J. Wu, W. C. Zhang, C. Wang, X. Qin, G. C. Liu, Z. X. Li and Y. Yu, *Sens. Actuators, B*, 2017, **245**, 615–621.
51 J. M. Goran, E. N. Phan, C. A. Favela and K. J. Stevenson, *Anal. Chem.*, 2015, **87**, 5989–5996.
52 L. L. Qu, Y. Y. Liu, S. H. He, J. Q. Chen, Y. Liang and H. T. Li, *Biosens. Bioelectron.*, 2016, **77**, 292–298.
53 F. Liu, T. Bing, D. Shangguan, M. Zhao and N. Shao, *Anal. Chem.*, 2016, **88**, 10631–10638.
54 Y. Xu, P. E. Pehrsson, L. Chen, R. Zhang and W. Zhao, *J. Phys. Chem. C*, 2007, **111**, 8638–8643.